Phototaxis Flight of Microdroplets in a Laser

Weizheng Cheng, Hanrui Zhu, Feiyu Zheng, Ben Chu, Ruitong Wang, Jinran Tao, Wanli Zhang, Peng Tao, Chengyi Song, Wen Shang, Benwei Fu,* and Tao Deng†

State Key Laboratory of Metal Matrix Composites, School of Materials Science and Engineering, Shanghai Jiao Tong University, Shanghai 200240, People's Republic of China

(Received 25 October 2022; revised 27 November 2023; accepted 24 January 2024; published 5 March 2024)

Phototaxis phenomenon is fundamental and critical for optical manipulation of micro-objects. Here, we report the size-dependent negative or positive phototaxis behaviors for microdroplets containing interfacial energy absorber flying in a laser. The critical diameters for such negative-to-positive turnover are studied through both experiments and simulation with different liquids and absorbers, which establishes the mechanism and reveals the role of both the liquid and the absorber inside the microdroplets. This study offers new insight for the manipulation of the phototaxis behavior of micro-objects, showing potential applications in optical trapping and transporting systems that involve light-microdroplet interactions.

DOI: 10.1103/PhysRevLett.132.104001

Droplet interaction with light is a ubiquitous phenomenon in various environments and systems. For instance, water droplets in clouds absorb and reflect sunlight in nature [1], and laser-tin droplet interaction produces plasma as an extreme ultraviolet source for lithography [2]. Light-droplet interactions involve a variety of physical and chemical processes (i.e., focusing and scattering of light by droplet, fragmentation of droplet via laser) [3,4], and have been widely studied in the field of meteorology, biology, and lithography.

Among these studies, one major interest of light-droplet interaction is the control of droplet movement by light. It has been reported that substances in light could exhibit phototaxis motion (move toward or away from the light source) via light-induced physical and chemical processes [5–7]. For instance, a laser changes the moving direction of droplet by inducing evaporation in different places on its surface [8], infrared light attracts liquid marble by locally adjusting its surface tension [9], and a Gaussian laser beam traps droplets through the force of radiation pressure [10]. These phenomena inspire the research of particle manipulation and motion control, and attract wide attention in the fields of droplet reactor, micromotor, drug delivery, etc. [11–14]. Here, we report another phototaxis phenomenon of microdroplet flight in a laser with a different mechanism. Through laser-microdroplet interaction, laser energy is deposited into a microdroplet and drives the microdroplet to move toward or away from the laser source. The diameters and components of microdroplets are essential to the distribution of laser energy deposition. The interfacial energy deposition and the induced interfacial evaporation play important roles in pulling microdroplets to the laser.

In the experiment, the microdroplets are first nebulized from either pure deionized water (DI) or graphene oxide (GO) nanofluid (GO 1 mg/mL dispersed in DI water), and then blown into a 1064-nm laser beam to interact with the laser (detailed experimental setup in Supplemental Material [15]). GO, which tends to spread at the air-water interface of microdroplets, is used to deposit laser energy at the interface [17,18]. The DI microdroplets with diameters of 8.1 and 2.0 μm are propelled away from the laser source, exhibiting negative phototaxis, as shown in Fig. 1(a), and so is the GO microdroplet with a diameter of 6.8 μm in Fig. 1(b). The GO microdroplet with a diameter of 2.2 μm, however, flies toward the laser source, showing positive phototaxis. Through statistical analysis of microdroplet flight in Fig. 1(c), we find that among all the DI and GO microdroplets, only GO microdroplets with diameters smaller than 3.0 μm exhibit positive phototaxis and fly toward the laser source while others fly with negative phototaxis. The visualization and the analysis above reveal that the diameter and the component play important roles in determining the moving direction of microdroplets.

In order to understand the motion of microdroplet, we divide it into acceleration and deceleration processes. When the laser is turned on with duration of 133 ns, the microdroplet is accelerated by the laser-microdroplet interaction. The interaction propels the microdroplet to move and gives it the initial velocity (v_0) and momentum (P_0) at the end of the acceleration process [Fig. 2(a)]. When the laser is off, which lasts as long as the laser pulse interval (about 1 ms), the microdroplet is decelerated to stop under the action of hydrodynamic force (F^h). On the microscale, gravitational force (F^g) has little effect on the motion of microdroplet [7], and is neglected for simplicity (detailed in Supplemental Material [15]). Here we apply Newtonian mechanics along the direction of laser propagation (z axis) to govern the deceleration process of the microdroplet:

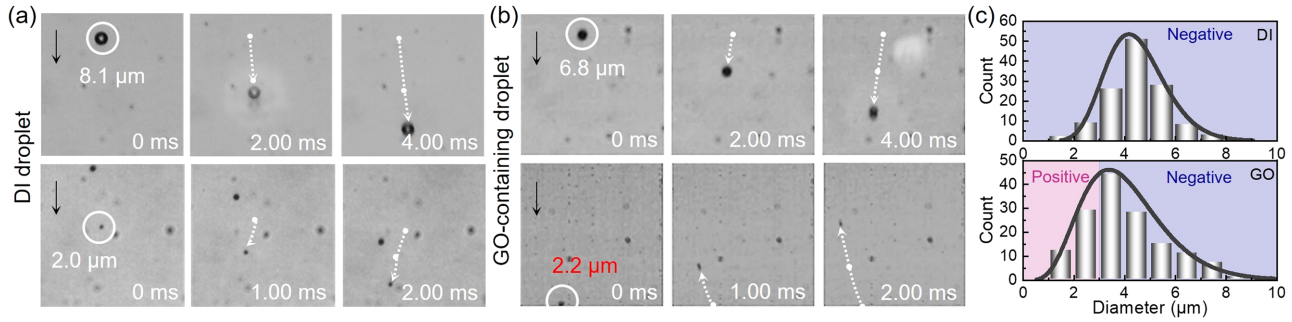

FIG. 1. Microdroplets flying toward and away from the laser. (a) Microdroplets of deionized water (DI) fly away from the laser source and exhibit negative phototaxis. (b) Microdroplets containing graphene oxide sheets show different flying behaviors. The larger one ($D \sim 6.8$ μm) flies away from the laser source (negative phototaxis), while the smaller one ($D \sim 2.2$ μm) flies toward the laser source (positive phototaxis). The black solid arrows in (a) and (b) indicate the direction of laser propagation. (c) Statistics of microdroplets with different diameters and components and their phototaxis behaviors. Only the GO microdroplets smaller than 3.0 μm in diameter show positive phototaxis.

$$m\frac{dv_z}{dt} = F_z^h, \tag{1}$$

where the hydrodynamic force is related to the viscosity of surrounding air (η) and microdroplet diameter (D): $F_z^h = -3\pi\eta D v_z$ [7]. v_z is the velocity of microdroplet along the z axis. As the deceleration process is long enough, the velocity of the microdroplet decreases to about zero at the end of the deceleration process, as shown in Fig. 2(a), and the conditions of velocity are given by $v_z(t = 0\ \text{ms}) = v_0$ and $v_z(t = 1\ \text{ms}) = 0$.

Solving Eq. (1), as detailed in the Supplemental Material [15], v_0 and P_0 of the microdroplet can be inferred from its displacement (Δz) and diameter (D) as $v_0 = 18\eta\Delta z/(\rho D^2)$ and $P_0 = 3\pi\eta D\Delta z$. Both v_0 and P_0 are proportional to Δz, and are related to the diameter by $v_0 \sim D^{-2}$ and $P_0 \sim D^1$. The calculation results of v_0 and P_0 are shown as surface plots in Figs. 2(b) and 2(c), and the experimental measurement of Δz and D are presented as dot plots. For DI microdroplets, their initial velocities are mainly distributed between 10^{-1} to 10^0 m/s. For GO microdroplets, the small ones ($D < 3.0$ μm) have positive phototaxis with initial velocities almost greater than 10^0 m/s, while the large ones ($D > 3.0$ μm) possess negative phototaxis with initial velocities of about 10^{-1} m/s. Figure 2(c) shows the initial momentum required for microdroplet flight. For small microdroplets ($D \sim 1.0$ μm), the initial momentum is about 10^{-15} Ns, while for large microdroplets ($D \sim 8.0$ μm), the required initial momentum is closer to 10^{-13} Ns. Through kinetic analysis, we infer v_0 and P_0 from D and Δz. These required v_0 and P_0 are obtained from the acceleration process by the laser-microdroplet interaction, which generates driving force and propels the microdroplets to move.

During the acceleration process, the laser illuminates and interacts with the microdroplet. The source laser used is an invisible infrared laser with a wavelength of 1064 nm. Bright sparks are, however, observed in the experiment as evidence of the laser-microdroplet interaction, which are generated by laser-induced optical breakdown [25,26]. When the laser passes through the microdroplet, the strong electromagnetic wave interacts with the water, causing the water molecule to release electrons and increasing the free electron density (FED, N_e) [27]. Once the FED reaches a critical value (N_e^{cri}), optical breakdown of water leads to the generation of brilliant plasma in space as shown in Figs. 1 and 2 [28,39]. The increased FED has a nonlinear absorption effect on the laser, and the water with high FED absorbs efficiently the laser energy and converts it into heat. To gain insight into the nonlinear absorption effect of FED on laser and the distribution of laser energy deposition to water, we simulate the laser-microdroplet interaction through numerical modeling (see Supplemental Material

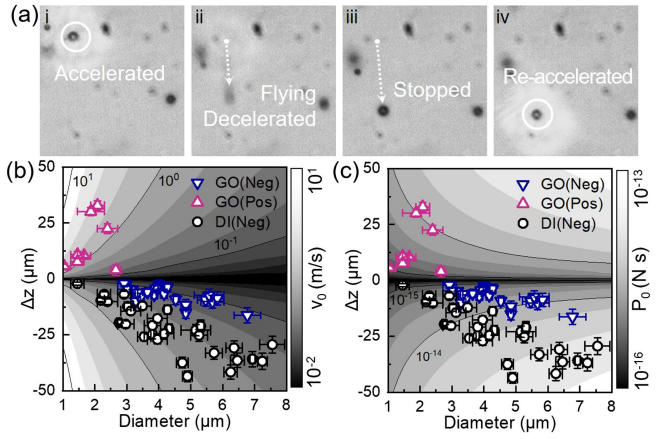

FIG. 2. Kinetic analysis of phototaxis flight of microdroplet. (a) Microdroplet flight is divided into an acceleration with the laser on (i) and a deceleration with the laser off (ii–iii), and a re-acceleration with the laser on again (iv). (b),(c) Initial velocity (b) and momentum (c) of the microdroplets obtained in stage (i). The scatter plot shows the experimental data, and the surface plot shows the result calculated according to Eq. (1).

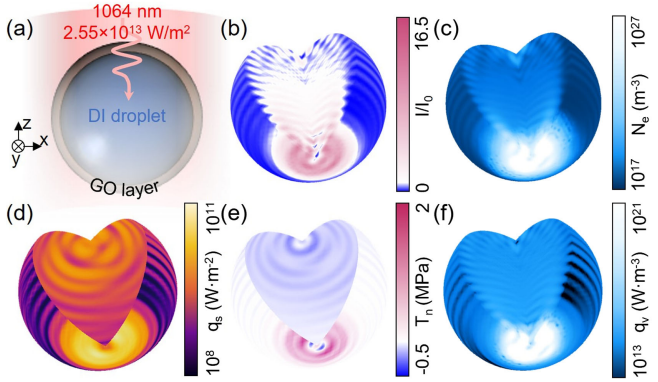

FIG. 3. (a) Schematic diagram of a laser beam acting on a GO microdroplet. (b)–(f) Distribution of laser intensity (b), free electron density (c), energy absorption of the GO layer at the air-water interface (d), pressure of laser radiation (e), and energy absorption of water in microdroplet (f) at the triggered state. The diameter of the microdroplet is 6 μm.

for details [15]). Because of the low surface energy of GO sheets, they tend to spread at the air-water interface [17,18], so the GO microdroplet is simplified as a water sphere covered by a thin GO layer, as shown in Fig. 3(a), with an effective thickness of the GO layer ($\tilde{d}_{\mathrm{GO}}$)

$$\tilde{d}_{\mathrm{GO}} = \frac{c_{\mathrm{GO}} V}{\rho_{\mathrm{GO}} A} = \frac{c_{\mathrm{GO}} D}{6\rho_{\mathrm{GO}}}, \tag{2}$$

where c_{GO}, ρ_{GO} are the concentration and the density of GO, and V,A are the volume and surface of the microdroplet. $\tilde{d}_{\mathrm{GO}}$ is diameter dependent as well. The DI microdroplet is viewed as a water sphere suspended in the air. The laser propagation (the field strength of electric field, $\vec{\mathrm{E}}$) is governed by Maxwell's equation in the frequency domain, and the growth of the free electron in water (the field of FED, N_e) is governed by a rate equation [1,34]. Relating the effective relative permittivity $\tilde{\epsilon}_r$ to N_e by

$$\tilde{\epsilon}_r(N_e) = \epsilon_r + \mathrm{i}\frac{\mathrm{e}^2 \tau_{\mathrm{e}} N_{\mathrm{e}}}{\omega \epsilon_0 m_e (1 - \mathrm{i}\omega\tau_e)}, \tag{3}$$

two governing equations are then coupled for modeling laser-microdroplet interaction, as detailed in the Supplemental Material [15]. Figures 3(b)–3(f) show the simulation results of a $6-\mu\mathrm{m}$ GO microdroplet when it reaches the triggered state. The triggered state is defined as when the maximal FED ($\mathrm{N_e^{max}}$) reaches a critical value ($\mathrm{N_e^{cri}} = 1.8 \times 10^{26}\ \mathrm{m}^{-3}$) [28,39]. When the light propagates through a microdroplet, the microdroplet acts as an optical condenser and has a focus effect on the light. Figure 3(b) shows the distribution and the enhancement of laser intensity inside the microdroplet (I/I_0) by the focus effect. It shows that the laser intensity inside the microdroplet is highly enhanced at the shadow face, and the maximal enhancement is 16.5 inside the 6-μm microdroplet ($I_{\mathrm{max}}/I_0 \sim 16.5$). This high laser intensity with strong energy results in violent interaction between the laser and the water at the enhanced area, and leads to rapid growth of free electron density (FED) of water [34,35], as shown in Fig. 3(c). The FED of water at the shadow face reaches the critical value at the same place where the laser intensity is highly enhanced. The FED has a nonlinear absorption effect on the laser, and when the FED is higher than $10^{24}\ \mathrm{m}^{-3}$, this effect becomes non-negligible [34,35]. As a result, other effects caused by laser-microdroplet interaction, such as energy deposition and irradiation, are affected by the increased FED [35]. Figures 3(d)–3(f) show the interfacial energy deposition, the optical pressure of laser irradiation, and the bulk energy deposition under the action of the FED. The variation of the microdroplet diameter would change the laser distribution and enhancement insides and thus affect the laser irradiation, the bulk energy deposition, and the interfacial energy deposition, as detailed in the Supplemental Material [15].

Based on the established model, we further evaluate the momentum induced by the laser-microdroplet interaction. The processes that provide momentum to the microdroplet include laser irradiation with radiation pressure, plasma expansion with plasma recoil force, and interfacial evaporation with vapor recoil force, as illustrated in Fig. 4(a). When the laser passes through the microdroplet, its propagating direction is changed by the curved gas-liquid interface, and its energy is partially absorbed by the microdroplet. The momentum lost by the laser along its propagating direction (P_z^l) is exchanged to the microdroplet and is expressed as

$$P_z^l(D) = \int \left(\iint T_n(D) n_z ds \right) dt \tag{4}$$

with $T_n(D)$ the radiation pressure and $\mathrm{n_z}$ the z-axis component of surface normal [36]. When laser-induced optical breakdown occurs, the generated plasma expands in space and pushes the microdroplet to move like launching a rocket [3,40]. Through the recoil of plasma expansion, the momentum (P_z^P) is exchanged between plasma and microdroplet along the moving direction (z axis) as

$$P_z^p(D) = \int \left(\iiint \frac{q_v(D)}{L^i} v^P n_z dV \right) dt, \tag{5}$$

with $q_v(D)$ the volume energy absorption of laser, L^i the latent heat of ionization for water, and v^P the expansion velocity (detailed in Supplemental Material [15]). In addition, in GO microdroplets, interfacial evaporation occurs on GO sheets. GO sheets at the gas-liquid interface absorb laser energy and convert it into heat, acting as interfacial heaters for evaporation. The GO layers with

different thicknesses ($\tilde{d}_{\mathrm{GO}}$) have different energy absorption and interfacial evaporation effects on the microdroplets [41,42]. Through the recoil of vapor departure, the momentum (P_z^v) is exchanged between vapor and microdroplet along the z axis as

$$P_z^v(D) = \int \left(\iint \frac{(q_s(D)/L^v)^2}{\rho} n_z ds \right) dt, \tag{6}$$

with $q_s(D)$ the interfacial energy absorption and L^v the latent heat of evaporation. Equations (4)–(6) relate P_z^l, P_z^P, and P_z^v to D through T_n, q_v, and q_s, which can be obtained through the modeling. Based on $T_n(D = 6\ \mu\mathrm{m})$ in Fig. 3(e), $q_v(D = 6\ \mu\mathrm{m})$ in Fig. 3(f), and $q_s(D = 6\ \mu\mathrm{m})$ in Fig. 3(d), it can be obtained that $\mathrm{P}_z^{\mathrm{l}}(D = 6\ \mu\mathrm{m}) = -35.3 \times 10^{-15}$ N s, $P_z^P(D = 6\ \mu\mathrm{m}) = 23 \times 10^{-15}$ N s, and $P_z^v(D = 6\ \mu\mathrm{m}) = 7.9 \times 10^{-15}$ N s.

Figure 4(b) shows the momentums of microdroplets obtained by the interaction of laser and microdroplet. The direction of the momentum generated by laser irradiation is the same as that of the laser propagation, tending to push the microdroplet away from the laser source, while the momentum of the microdroplet generated by plasma expansion and interfacial evaporation are in the opposite direction, pulling the microdroplet to the laser. The absolute values of the momentums show that for microdroplets larger than 3 μm, the effect of light radiation is greater than those of plasma expansion and interfacial evaporation. For microdroplets smaller than 3 μm, the interfacial evaporation plays an essential role. We sum these three momentums to evaluate the combined effect of laser irradiation, plasma expansion, and interfacial evaporation on microdroplet flight. For GO microdroplets, the total momentum along the z axis is

$$P_z^{\mathrm{tot}} = P_z^l + P_z^p + P_z^v. \tag{7}$$

For DI microdroplets, due to the lack of GO sheets, interfacial evaporation has a very small effect on DI microdroplets since there is no interfacial energy absorber (GO sheets) at the liquid-gas interface of the pure DI water microdroplet [42,43]. Thus, P_z^v from the interfacial evaporation in Eq. (7) is negligible for DI microdroplet. Figure 4(c) shows the total momentums of the DI and GO microdroplets, which are in good agreement with the initial momentum from the experimental data in Fig. 2(c). The results show that for the DI microdroplets with all diameters and the GO microdroplets with diameters larger than 3.0, the combined effect of three momentums gives a negative propelling direction and tends to push the microdroplet away from the laser source. This combined effect for the negative phototaxis of the DI microdroplet and large GO microdroplet ($D > 3$ μm) is due to the domination of laser irradiation, as shown in Fig. 4(b). For the small GO microdroplet ($D < 3$ μm), the combined effect

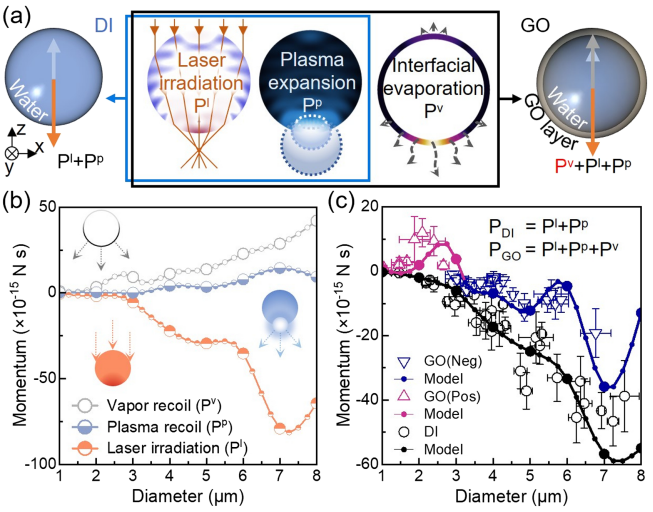

FIG. 4. (a) Illustration of momentum that microdroplets gain from laser irradiation, plasma expansion, and interfacial evaporation. (b) Momentums of microdroplets with 0.25-μm interval. The data with 1-μm interval (large symbols) correspond to results in Fig. 5 in the Supplemental Material [15]. (c) The combined effect of three processes on the momentum of the microdroplet and comparison of modeling values with experimental estimation in Fig. 2(c).

provides a positive propelling direction and pulls them toward the laser source. As shown in Fig. 4(b), for the small GO microdroplet ($D < 3$ μm), the pulling effect of interfacial evaporation is dominant.

For the GO microdroplet, the transition of the total momentum at $D = 3.0$ μm indicates that the moving direction of the GO microdroplet would be turned over at $D = 3.0$ μm. In the experiment, we observed that the GO microdroplet flies from negative to positive phototaxis as its diameter decreases from 4.2 to 2.0 μm (see Supplemental Material [15], movie 1). Its flying direction transition occurs at $D = 3.0$ μm, as shown in Fig. 5, which is in good agreement with the prediction above. For the microdroplet with such turnover behavior, there is a solution (critical diameter) for the zero value of total momentum:

$$D_{\mathrm{cri}} = f^{-1}(P_z^{\mathrm{tot}} = 0), \tag{8}$$

with f^{-1} the inverse function of $P_z^{\mathrm{tot}} = f(D)$. $f(D)$ is a general form that summarizes the relation from D to P_z^{tot}, as shown in Fig. 4(c), and its detailed form is given by Eqs. (14)–(27) in the Supplemental Material [15].

Based on the numerical modeling above, we quantitatively analyze the combined effect of laser irradiation, plasma expansion, and interfacial evaporation, and reveal the mechanism of the diameter- and component-dependent phototaxis flight of the microdroplet. The component inside the microdroplet acts as an interfacial energy absorber and plays the key role in interfacial evaporation, and interfacial

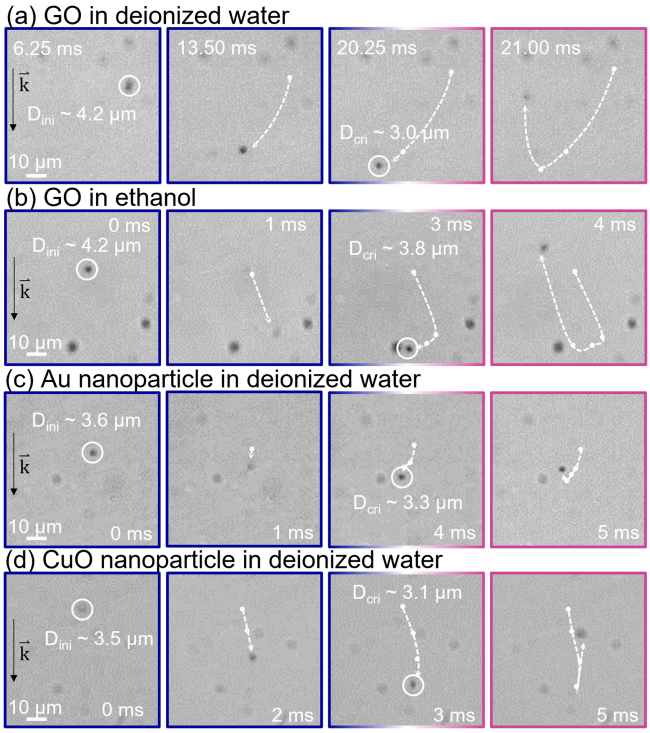

FIG. 5. (a) A GO microdroplet reverses its phototaxis at 3.0 μm. (b)–(d) The turnover motions are also observed using GO-ethanol nanofluid, Au-water nanofluid, and CuO-water nanofluid.

evaporation is essential to pull the microdroplet to the laser. To generalize the reported phototaxis phenomenon and the proposed mechanism, we varied the nanofluids (GO-ethanol nanofluid, Au-water nanofluid, and CuO-water nanofluid), and the similar phenomena were observed, as shown in Figs. 5(b)–5(d) and Fig. S7 [15].

In summary, this work reports the phototaxis flights of microdroplet under the combined effect of laser-microdroplet interaction. A model of laser-microdroplet interaction is established to explore the effects of laser-microdroplet interaction on the phototaxis flight of the microdroplet. The diameter of the microdroplet is essential for the distribution of laser energy deposition, and the component inside microdroplet is determinative for interfacial energy deposition. This work reveals that laser irradiation pushes the microdroplet away from the laser while interfacial evaporation plays the key role in pulling the microdroplet to the laser. The reported phototaxis phenomenon of the microdroplet can be extended to other nanofluids and provide an effective approach for manipulating the micro-object at microscale, showing potentials in optical trapping and transporting systems.

We acknowledge the funding support from National Key R&D Project from Ministry of Science and Technology of China (Grant No. 2022YFA1203100), National Natural Science Foundation of China (Grants No. 52302104, No. 51873105, and No. 51973109), and Innovation Program of Shanghai Municipal Education Commission (Grant No 2019-01-07-00-02-E00069). We also acknowledge the Center of Hydrogen Science of Shanghai Jiao Tong University, the Instrumental Analysis Center, and the Zhiyuan Innovative Research Center of Shanghai Jiao Tong University for their support.

*Corresponding author: fuwei880603@sjtu.edu.cn
†Corresponding author: dengtao@sjtu.edu.cn

[1] C. Zhang, M. Tang, H. Zhang, and J. Lu, Opt. Express **27**, 8456 (2019).
[2] O. O. Versolato, Plasma Sources Sci. Technol. **28**, 083001 (2019).
[3] A. L. Klein, W. Bouwhuis, C. W. Visser, H. Lhuissier, C. Sun, J. H. Snoeijer, E. Villermaux, D. Lohse, and H. Gelderblom, Phys. Rev. Appl. **3**, 044018 (2015).
[4] C. Zensen, I. E. Fernandez, O. Eickelberg, J. Feldmann, and T. Lohmuller, Adv. Sci. (Weinh.) **4**, 1600238 (2017).
[5] D. Zhang, Y. Sun, M. Li, H. Zhang, B. Song, and B. Dong, J. Mater. Chem. C **6**, 12234 (2018).
[6] X. Zhang, Q. Fu, H. Duan, J. Song, and H. Yang, ACS Nano **15**, 6147 (2021).
[7] A. J. Bae, D. Hanstorp, and K. Chang, Phys. Rev. Lett. **122**, 043902 (2019).
[8] S. An, M. Zhu, K. Gu, M. Jiang, Q. Shen, B. Fu, C. Song, P. Tao, T. Deng, and W. Shang, Nanoscale **12**, 4295 (2020).
[9] L. Xu, C. Ma, B. Guan, J. Lin, K. Xiong, F. Mou, M. Luo, and J. Guan, Appl. Mater. Today **19**, 100595 (2020).
[10] A. Ashkin, Phys. Rev. Lett. **24**, 156 (1970).
[11] K. Dietrich, N. Jaensson, I. Buttinoni, G. Volpe, and L. Isa, Phys. Rev. Lett. **125**, 098001 (2020).
[12] D. McGloin, Rep. Prog. Phys. **80**, 054402 (2017).
[13] D. R. Link, S. L. Anna, D. A. Weitz, and H. A. Stone, Phys. Rev. Lett. **92**, 054503 (2004).
[14] Y. Wei, G. Cheng, H. P. Ho, Y. P. Ho, and K. T. Yong, Chem. Soc. Rev. **49**, 6555 (2020).
[15] See Supplemental Material at http://link.aps.org/supplemental/10.1103/PhysRevLett.132.104001 for details on the experimental process, theoretical estimation, and numerical modeling, which includes Refs. [16–38].
[16] D. W. Pang, F. W. Yuan, Y. C. Chang, G. A. Li, and H. Y. Tuan, Nanoscale **4**, 4562 (2012).
[17] F. Guo, M. Creighton, Y. Chen, R. Hurt, and I. Kulaots, Carbon **66**, 476 (2014).
[18] F. Guo, F. Kim, T. H. Han, V. B. Shenoy, J. Huang, and R. H. Hurt, ACS Nano **5**, 8019 (2011).
[19] S. Chandrasekhar, Rev. Mod. Phys. **15**, 1 (1943).
[20] C. Jones, M. Gomez, R. M. Muoio, A. Vidal, R. A. Mcknight, N. D. Brubaker, and W. W. Ahmed, Phys. Rev. E **103**, 032403 (2021).
[21] J. Mo and M. G. Raizen, Annu. Rev. Fluid Mech. **51**, 403 (2019).
[22] S. Shiri, S. Sinha, D. A. Baumgartner, and N. J. Cira, Phys. Rev. Lett. **127**, 024502 (2021).
[23] J. C. Padrino, J. E. Sprittles, and D. A. Lockerby, J. Fluid Mech. **862**, 312 (2019).
[24] J. B. Young, Aerosol Sci. Technol. **45**, 927 (2011).

[25] Y. E. Geints, A. M. Kabanov, G. G. Matvienko, V. K. Oshlakov, A. A. Zemlyanov, S. S. Golik, and O. A. Bukin, Opt. Lett. **35**, 2717 (2010).
[26] A. L. Klein, C. W. Visser, W. Bouwhuis, H. Lhuissier, C. Sun, J. H. Snoeijer, E. Villermaux, D. Lohse, and H. Gelderblom, Phys. Fluids **27**, 091106 (2015).
[27] C. A. Sacchi, J. Opt. Soc. Am. B **8** (1991).
[28] F. H. Loesel, M. H. Niemz, J. F. Bille, and T. Juhasz, IEEE J. Quantum Electron. **32**, 1717 (1996).
[29] A. Vogel *et al.*, Appl. Phys. B **68**, 271 (2014).
[30] N. Linz, S. Freidank, X.-X. Liang, and A. Vogel, Phys. Rev. B **94**, 024113 (2016).
[31] N. Linz, S. Freidank, X.-X. Liang, H. Vogelmann, T. Trickl, and A. Vogel, Phys. Rev. B **91**, 134114 (2015).
[32] L. Keldysh, Sov. Phys. JETP **20**, 1307 (1965).
[33] A. Rudenko, P. Rosenow, V. Hasson, and J. V. Moloney, Optica **7**, 115 (2020).
[34] A. Rudenko and J. V. Moloney, Adv. Photonics Res. **1**, 2000029 (2020).
[35] A. Rudenko, J.-P. Colombier, and T. E. Itina, Int. J. Numer. Model. **31**, e2115 (2018).
[36] O. G. Helleso, Appl. Opt. **56**, 3354 (2017).
[37] S. Okada, S. Ohsaki, H. Nakamura, and S. Watano, Chem. Eng. Sci. **227**, 115938 (2020).
[38] Y. E. Geints, A. A. Zemlyanov, and R. L. Armstrong, Appl. Opt. **33**, 5805 (1994).
[39] M. H. Niemz, Appl. Phys. Lett. **66**, 1181 (1995).
[40] R. G. Pinnick, A. Biswas, R. L. Armstrong, S. G. Jennings, J. D. Pendleton, and G. Fernaandez, Appl. Opt. **29**, 918 (1990).
[41] J. T. Robinson, S. M. Tabakman, Y. Liang, H. Wang, H. S. Casalongue, D. Vinh, and H. Dai, J. Am. Chem. Soc. **133**, 6825 (2011).
[42] P. Tao, G. Ni, C. Song, W. Shang, J. Wu, J. Zhu, G. Chen, and T. Deng, Nat. Energy **3**, 1031 (2018).
[43] H. Ghasemi, G. Ni, A. M. Marconnet, J. Loomis, S. Yerci, N. Miljkovic, and G. Chen, Nat. Commun. **5**, 4449 (2014).